

GEOTECHNICAL CONSIDERATIONS ASSOCIATED WITH THE POATINA POWER STATION CAVERN

David Sainsbury¹, Kevin Stacey², Bre-Anne Sainsbury³ and Peter Hills⁴

¹Geotechnica, Melbourne; ²Hydro Tasmania, Hobart, ³Deakin University, Waurn Ponds, ⁴Pitt & Sherry, Hobart

<https://doi.org/10.56295/AGJ5745>

ABSTRACT

The Poatina Power Station Cavern was designed with a focus on the newly emerging rock mechanics theory and principles that were rapidly developing during the 1950's and 60's. This included measurement of the in-situ rock mass stress condition and photo-elastic analysis of the induced stress around the planned underground openings. These studies led to the adoption of many 'firsts' in rock mechanics that included a trapezoidal roof shape, installation of stress relieving slots and fully encapsulated grouted rebar bolts. Based on historical documentation of the construction of the cavern, a three-dimensional numerical model of the cavern construction sequence has been developed. The model is able to provide an accurate match to the observed and monitored ground conditions during construction that includes observed failure modes and instrumentation data. Based on the calibrated model outcomes, Hydro Tasmania was able to undertake a more informed review of the risks associated with the current and future ground support capacity and were able to reliably assess rehabilitation requirements for the cavern support system.

1 INTRODUCTION

The 363 MW Poatina Underground Power Station, in north-central Tasmania, forms part of Hydro Tasmania's Vingina / Great Lake - South Esk Hydro-Electric Scheme. Preliminary construction work on the cavern commenced in late 1957 and the power station was officially opened in March 1965. A detailed description of the engineering design, rock mechanics studies and observations during excavation of the 91.4 m long, 13.7 m wide and 25.9 m high machine hall cavern have been provided by Colebatch et al. (1959), Colebatch et al. (1963); Endersbee and Hofto (1963) and Ballantine et al. (1965). Figure 1 illustrates the final cavern design arrangement.

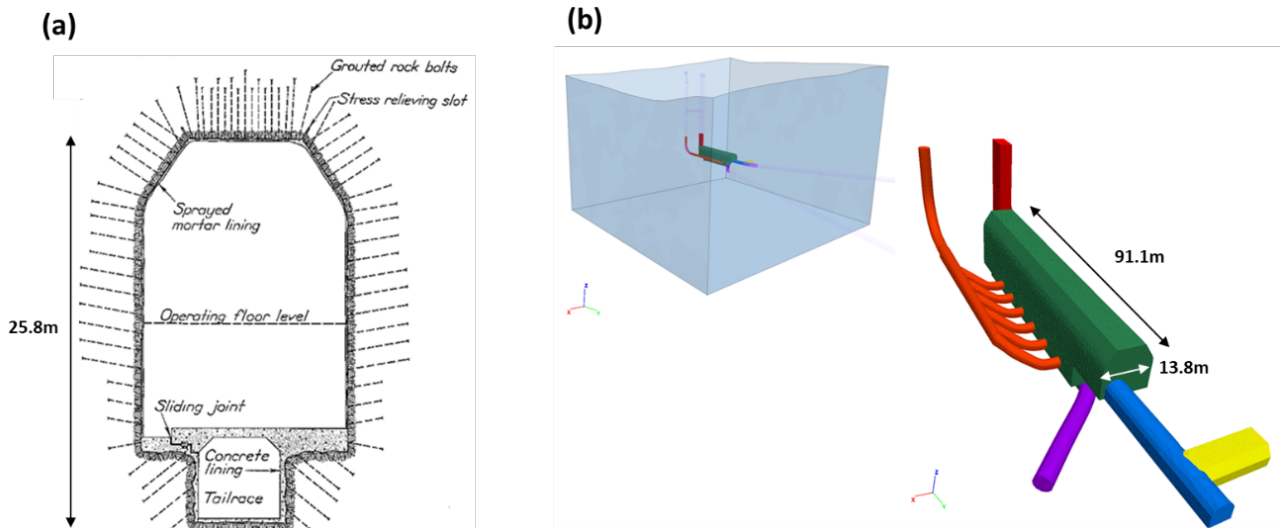


Figure 1: a) Design cross-section (Endersbee and Hofto, 1963) b) Cavern dimensions and limits of 3DEC model

The Poatina cavern was designed with a focus on the emerging rock mechanics theory and principles that were rapidly developing during the 1950's and 60's. This included measurement of in-situ rock mass stress and photo-elastic analysis of stresses around the planned underground openings (Worotnicki, 1961; Endersbee and Hofto, 1963). These studies led to the adoption of a trapezoidal roof shape which formed the roof of the cavern. Furthermore, photo-elastic stress studies deemed it necessary to drill stress relief holes along the intersection between the flat roof and the inclined upper wall of the arch, as illustrated in Figure 2 (Endersbee and Hofto, 1963). These closely spaced stress relief holes were installed to provide a "plastic hinge" that minimised the stresses in the arch (Dickinson and Gerrard, 1963).

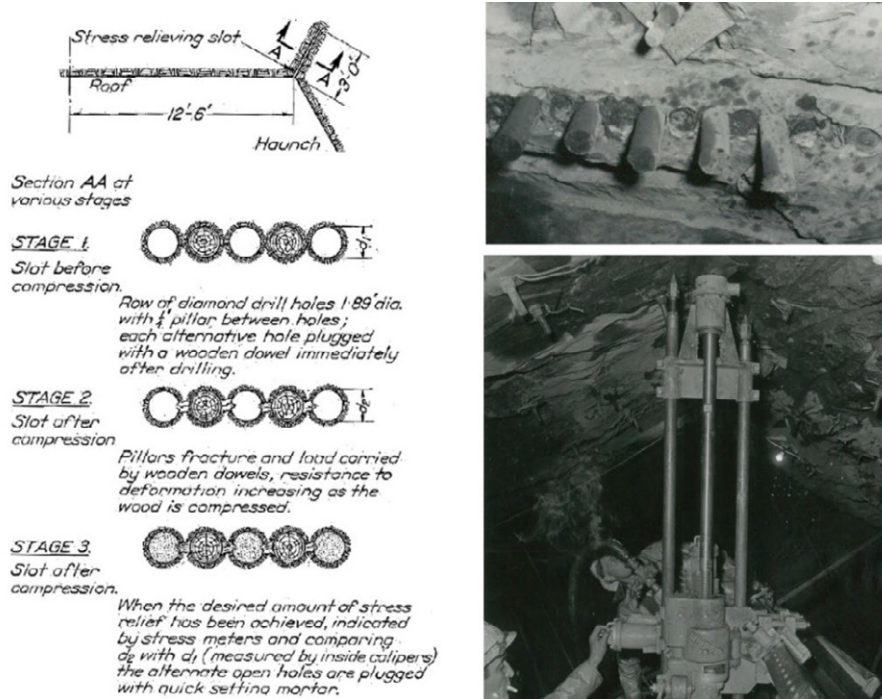


Figure 2: Stress relieving procedure after Endersbee and Hofto (1963)

Support of the cavern consists of grouted rock bolts, steel mesh and 100mm thick sprayed shotcrete - illustrated in Figure 3. The mechanical, end-anchored, slot and wedge type rock bolts developed and implemented by the Hydro-Electric Commission of Tasmania and the Snowy Hydro Hydro-Electric Authority (Pender, Hosking and Mattner, 1963) are some of the earliest reported use of rock bolts for permanent support in underground civil construction. The bolts were intended to have full grout encapsulation to provide long-term corrosion protection, although there is evidence at Poatina and elsewhere, that the methodology adopted for grouting was not effective.

Since the design and construction of the cavern, the stability of the excavation and its ground support elements have not been assessed to determine cavern stability and ground support requirements based on current day best-practice rock mechanics techniques. This paper outlines the numerical analysis that was completed using the discontinuum, three-dimensional distinct element code 3DEC (Itasca Consulting Group, 2022) to determine the current and future Factor of Safety of the cavern.

Discontinuum modelling techniques provide significant insight and understanding to rock mechanics processes that are not possible to test with continuum modelling approaches (Fairhurst, 2006). For this reason, recent best-practice numerical analysis of large hydropower cavern complexes such as the Sardar Sarovar and Tehri Caverns (Dasgupta, 2000), Shenxu Caverns (Zhang et al. 2016,.) Baihetan Caverns (Cui et al., 2016; Tang et al., 2019; Li et al., 2020; Hu et al., 2020), Siah Bisheh Cavern (Ghorbani and Sharifzadeh, 2009; Yazdani et al., 2012) have all used 3DEC to assess cavern stability.

2 GEOTECHNICAL AND MODELLING PARAMETERS

2.1 GEOMECHANICAL PROPERTIES

The Poatina cavern is situated at 150 m depth within a sequence of Permian mudstones. The roof of the cavern is in the Brumby Formation which is a thinly bedded highly fossiliferous calcareous mudstone (marl). The main body of the cavern is situated in the Quamby Formation which is a massive mudstone with occasional thin bands of shale (Endersbee and Hofto, 1963; Colebatch et al., 1959).



Figure 3: Poatina cavern during construction

Based on the descriptions of the mudstones, two scales of strength anisotropy can be defined that need to be accounted for in the numerical analysis. Figure 4 presents examples of the thinly bedded nature of the Brumby and Quamby mudstones which result in anisotropic strength and deformation behaviour of the rock mass at the cavern scale.

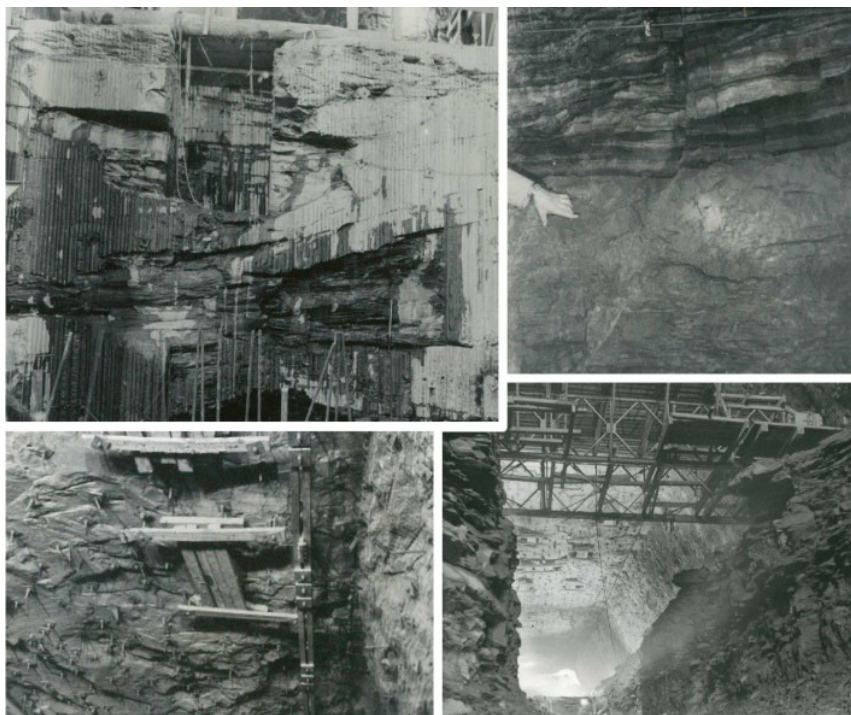


Figure 4: Thinly bedded nature of the Brumby and Quamby mudstone

Explicit structures that can slip and separate were defined to represent this regional scale anisotropy. The bedding planes were simulated with 100 percent persistence and spacing of 0.5 m with a standard deviation of 0.1 m based on visual observations by the authors. The geological setting and its representation in the numerical model are illustrated in Figure 5.

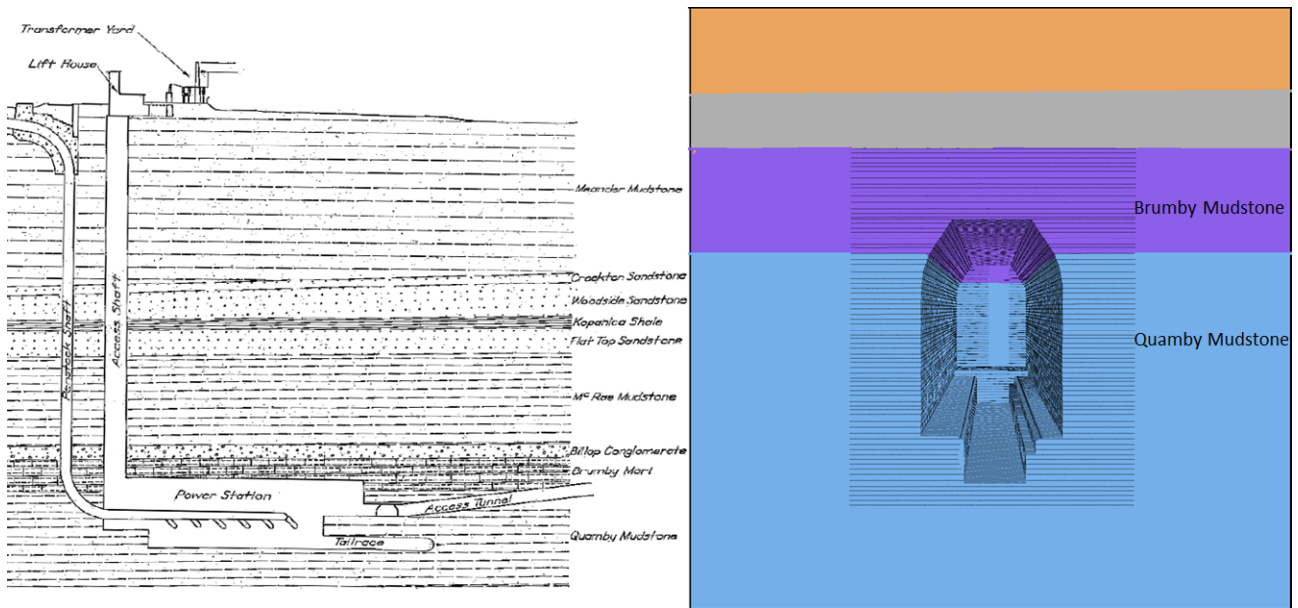


Figure 5: Geological setting (Endersbee and Hofto, 1963) and explicit bedding planes simulated in 3DEC

Table 1 presents the shear strength parameters assigned to them. The properties were determined based on a back-analysis of their response within the numerical model during early stages of excavation (as described in Section 3.1.1).

Table 1: Explicit structure properties

Kn [Pa/m]	Ks [Pa/m]	Cohesion [kPa]	Residual Cohesion [kPa]	Friction [deg.]	Tension [MPa]	Dilation [deg.]
2e10	2e9	50	10	30	0	5

Local scale anisotropy, that is characterised by a smaller scale, intact/rock block response has been determined based on laboratory testing presented by Endersbee and Hofto (1963) – summarised in Table 2.

Table 2: Intact rock parameters

	σ_c [MPa]	E [GPa]	ν
Brumby Mudstone	34 - 41	40	0.13
Quamby Mudstone	55 - 65	35	0.2

For this local response, a ubiquitous joint modelling approach has been adopted to represent the anisotropic rock mass behaviour (Sainsbury and Sainsbury, 2017b; Kazakidis and Diederichs, 1993, Clark, 2006; Sainsbury, 2017). A series of large-scale (4 m high) simulated compression tests have been conducted within 3DEC (Itasca Consulting Group, 2022) to simulate the anisotropic behaviour. To account for the significant impact that micro-flaws (pores, open cracks, veins) and weathering/alteration can have on the strength scale effect, the rock block strength was assigned to be 80 percent of the laboratory unconfined compressive strength reported by Endersbee and Hofto (1963). This value is based on an empirical scale effect relation for intact rock developed by Hoek and Brown (1997) and extended by Yoshinaka et al. (2008).

The ubiquitous joint cohesion and friction angles of 50 kPa and 26° were assigned based on descriptions of the mudstones (Pike et al., 1966; Clarke, 1968) and in situ observations by the authors. In order to develop anisotropic rock mass strengths, a series of UCS and triaxial ($\sigma_3 = 2$ MPa) tests were simulated with β angles from 0° to 90°. Figure 6 illustrates the resulting U-shaped anisotropic strength curve with continuous variability for the mudstones, while Figure 7 presents the simulated stress-strain response from the Brumby mudstone specimens with β angles of 0°, 60° and 80°. Loading perpendicular to bedding ($\beta = 0^\circ$) results in a stiff, brittle response as shear failure of the matrix dominates the failure mechanism. Sliding along the ubiquitous joints at a β angle of 60° results in a weak, ductile loading response. The resulting ubiquitous joint input properties are presented in Table 3.

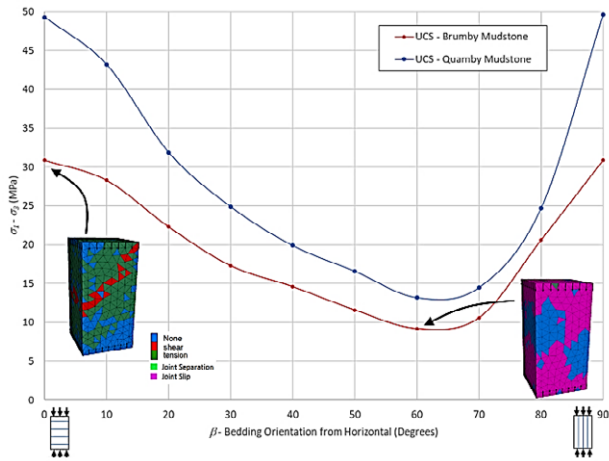


Figure 6: U-shaped anisotropic strength curve with continuous variability for the simulated material

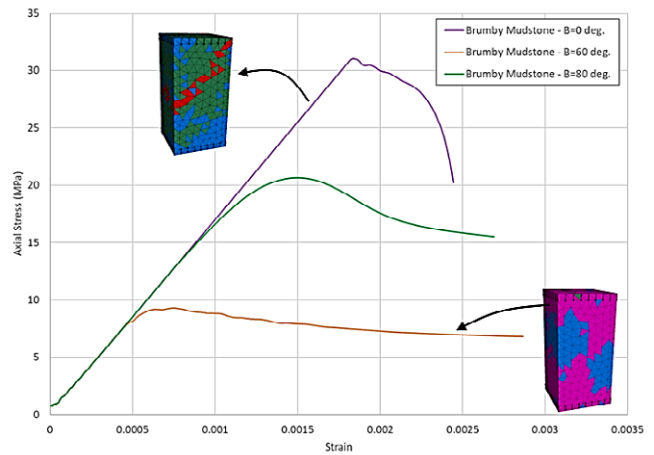


Figure 7: Stress-strain response of simulated Brumby Mudstone rock block specimens

Table 3: Calibrated ubiquitous joint properties

	E [GPa]	ν	Matrix Properties			Ubiquitous Joint Properties	
			c_p [MPa]	ϕ_p [deg]	σ_i [MPa]	c_p [MPa]	ϕ_p [deg]
Brumby Mudstone	17	0.23	6.4	44.6	0.64	1.9	35
Quamby Mudstone	22	0.23	10.0	45.7	1.0	3.0	35

The implementation of both scales of strength anisotropy within the model is presented in Figure 8.

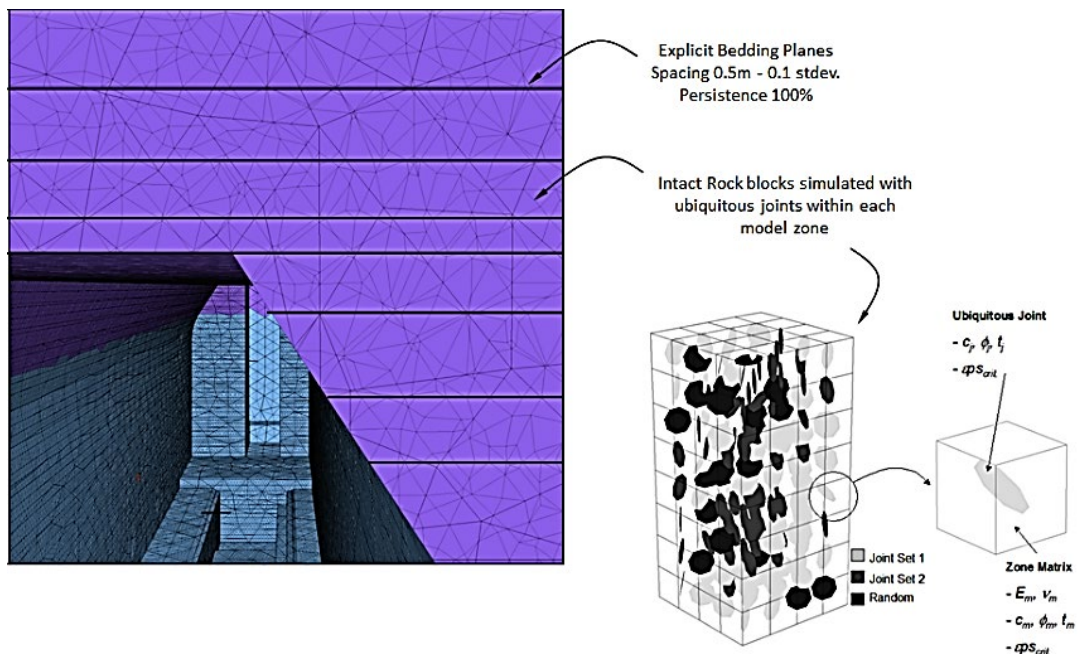


Figure 8: Model discretisation (modified after Sainsbury, 2008)

2.2 IN-SITU STRESS

There is significant uncertainty regarding the in-situ stress regime in the vicinity of the Poatina cavern. Stress measurements aligned with the cavern axis at the distributor gallery level were initially reported by Worotnicki (1961). Refinements to these measurements as reported by Endersbee and Hofto (1963) and summarised in Table 4 have been assigned in the model.

Table 4: In-situ Stress Regime (after Endersbee and Hofto, 1963)

Stress	Magnitude [MPa]
Vertical	8.5
Perpendicular to cavern axis	16.5
Parallel to cavern axis	12.4

2.3 GROUND SUPPORT

2.3.1 Rock bolts

The slot and wedge rock bolts installed throughout the Poatina cavern have been simulated with the in-built hybrid bolt structural element logic within 3DEC. The placement of bolts within the model was simulated in-cycle to ensure an accurate load-path is followed during sequential excavation and bolting. Figure 9 illustrates the distribution of bolts at completion of the cavern.

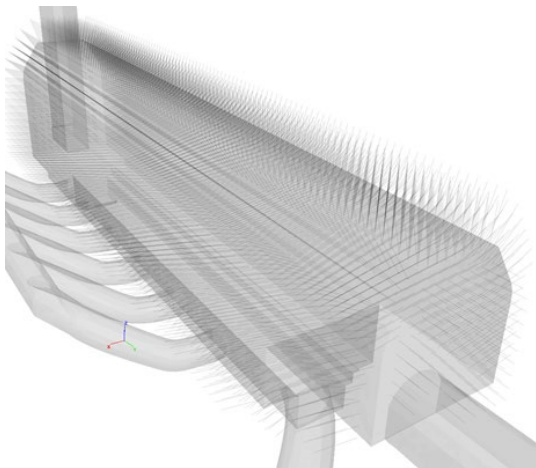


Figure 9: Rock bolts simulated within the 3DEC model

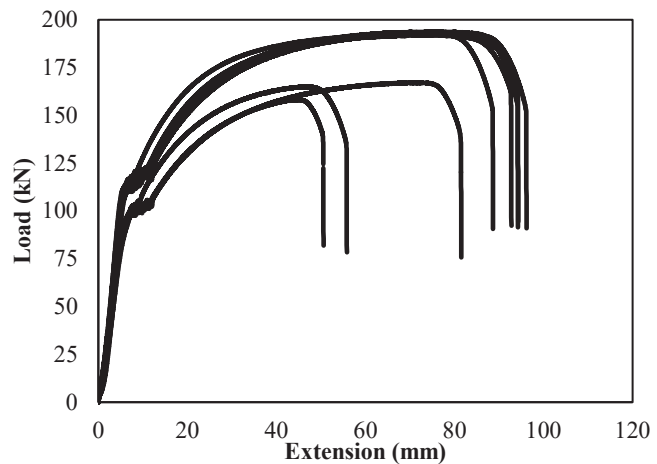


Figure 10: Tensile load versus extension of rebar bolts retrieved from Poatina Cavern

Table 5 presents the mechanical properties of the hybrid bolts applied in the model. In relation to properties of the steel, Colebatch et al. (1963) reported a failure load between 170-210 kN. This capacity is consistent with recent mechanical tension testing of the bolts retrieved from the cavern presented in Figure 10. Furthermore, recent pull-testing of bolts within the roof of the cavern have all returned at least 100 kN capacity with some bolts pulled to failure at 175 kN. These results are consistent with pull-out tests on slot and wedge anchors elsewhere (Thompson and Villaescusa, 2014; US Army Corps of Engineers, 1980; Moy, 1975).

To confirm the implementation of the bolt properties within the model, a series of simulated pull tests were conducted. Bolts modelled with full grout encapsulation reached the full capacity of the steel rebar, while bolts without encapsulation slipped at the simulated anchor capacity of 40 kN, as illustrated in Figure 11.

Table 5: Slot and wedge bolt properties

	Modulus [GPa]	Axial Yield Strength [kN]	Axial Yield Strain	Grout Strength [kN/m]	Grout Stiffness [kN/m/m]	Shear Strength [kN/m]	Shear Stiffness [kN/m/m]	Shear Strain
Bolt (23.4 mm) dia.	182	150	0.03	100	500	120	1000	0.01
Anchor	182	150	-	400	1000	-	-	-

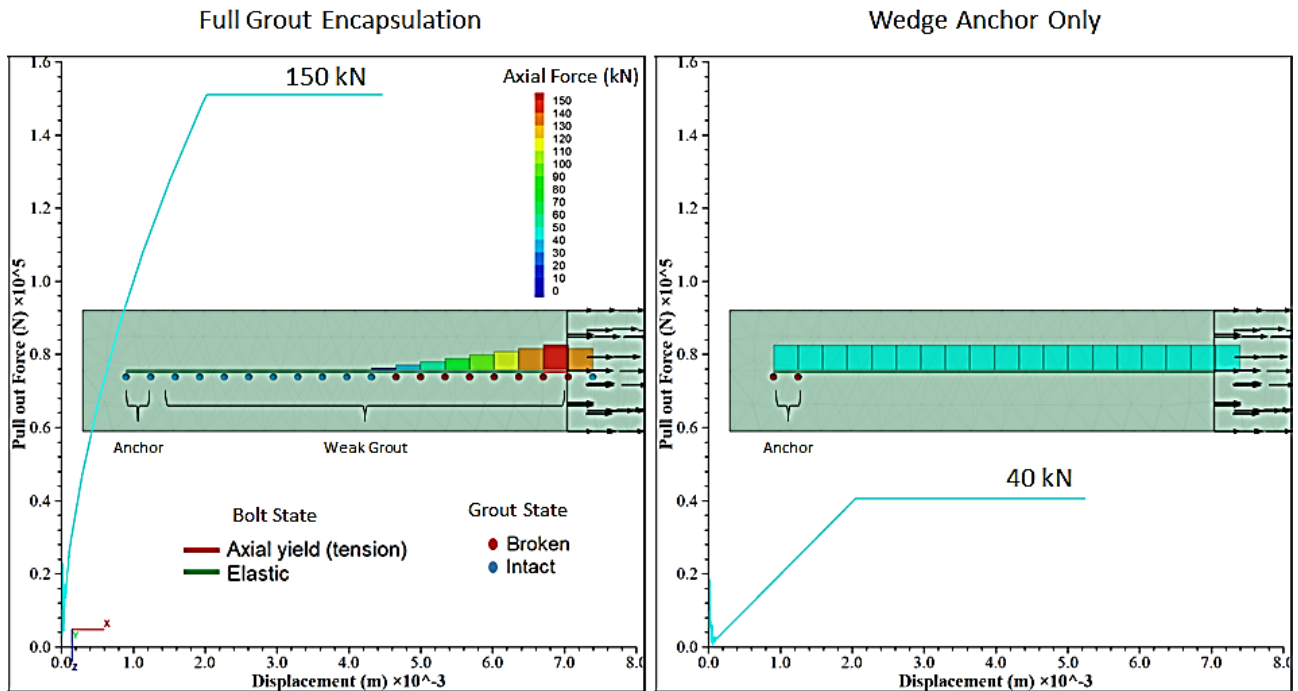


Figure 11: Simulated pull test results

2.3.2 Shotcrete (gunite) liner

During construction, a 100 mm thick, sprayed shotcrete (gunite) liner was applied over 75 mm x 75 mm, 10-gauge mesh after complete excavation of the top heading and first two benches.

The liner was simulated in 3DEC using the in-built liner structural element logic. It was installed progressively, with its stiffness and strength progressively increased to represent, as close as possible, its placement sequence and resulting ground/support interaction within the cavern. The material properties used to simulate the liner are presented in Table 6. These values have been estimated based on Endersbee and Hofto (1963) and properties of typical mesh and shotcrete composites (Barros, 1998).

Table 6: Shotcrete liner material properties

Modulus [GPa]	ν	K_n [Pa/m]	K_s [Pa/m]	Cohesion [MPa]	Friction [deg.]	Tension [MPa]
15	0.15	1e9	1e9	0.5	60	1

3 NUMERICAL ANALYSIS

3.1 ROCK RESPONSE TO EXCAVATION

In order to provide confidence in the model response, a series of comparisons have been completed based on in-situ observations during excavation and the model response. These comparisons include both the rock mass and ground support response to the excavation process. A summary is provided below.

3.1.1 Crown Drive behaviour

An initial excavation (1.5 m wide x 2.1 m high exploratory crown drive) without support prior to implementing the trapezoidal cavern roof profile design was completed. Figure 12 illustrates the exploratory crown drive location within the cavern geometry.

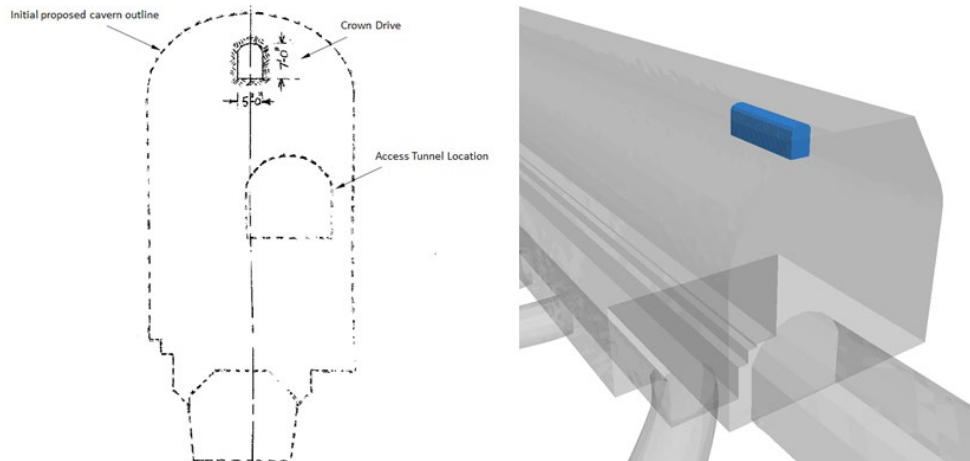


Figure 12: Geometry of exploratory crown drive

During excavation of the exploratory crown drive, progressive fracturing of the roof rock mass in large thin slabs was experienced (Endersbee and Hofto, 1963), as illustrated in Figure 13, and is observed to be localised on the first horizontal bedding parting in the roof. Figure 14 presents the simulated response of this drive in the model. The model is shown to accurately simulate the observed failure mechanism/s within the crown drive which is controlled by tensile separation of the ubiquitous joints within the immediate roof bed (indicated by joint separation in the plasticity state). The roof instability is terminated at the first explicit bedding parting within the roof as observed by the model displacements and velocities.



Figure 13: Slabbing in the roof of the unsupported crown drive (Endersbee and Hofto, 1963)

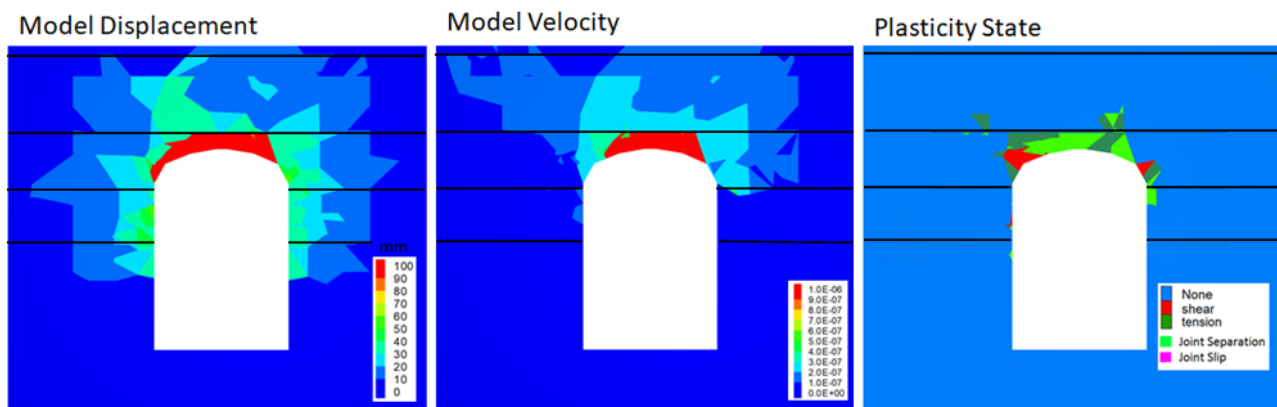


Figure 14: Model response on a cross-section through the crown drive

As a result of this matched failure mode and general state of the surrounding rock mass around the crown drive, it can be concluded that the model is a reasonable representation of the in-situ conditions during initial construction and suitable for simulation of the full cavern response.

3.1.2 Cavern response

Excavation of the Poatina cavern was simulated with a 6 m advance followed by placement of rock bolts 2 m behind the face. The excavation and support sequence was simulated to match the as-built sequence presented in Figure 15.

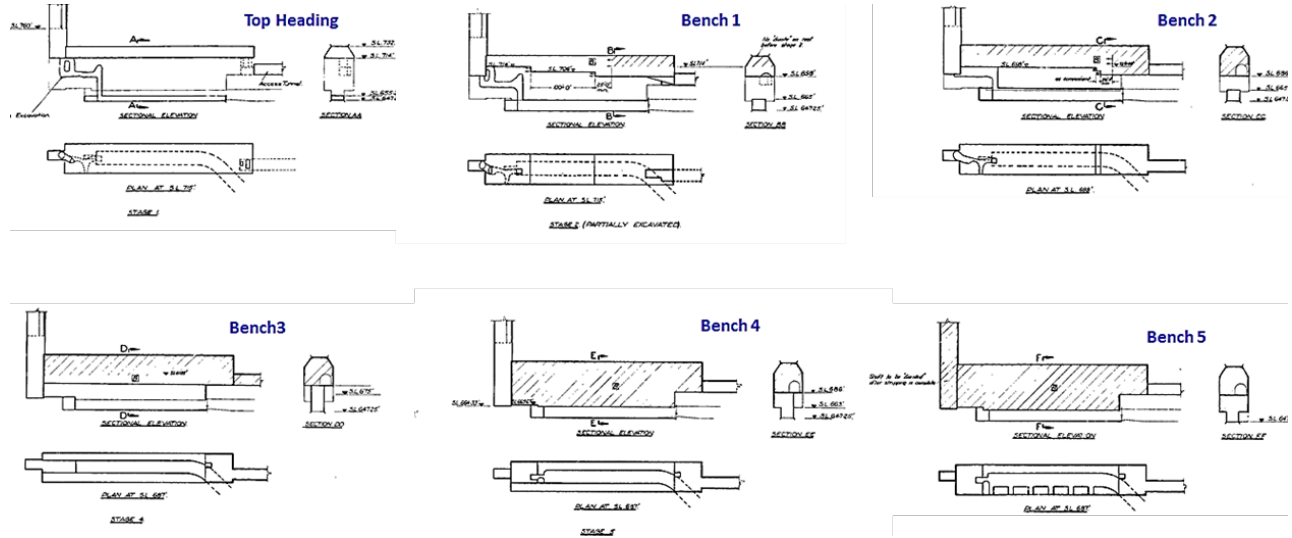


Figure 15: As-built excavation and support sequence (The Hydro-Electric Commission, Tasmania, A7819)

Monitoring instrumentation installed during excavation included flat jacks, convergence pins and ungrouted bolts for measuring dilation. Figure 16 illustrates the location of the monitoring instrumentation installed throughout the cavern that have been used as verification points for the model results.

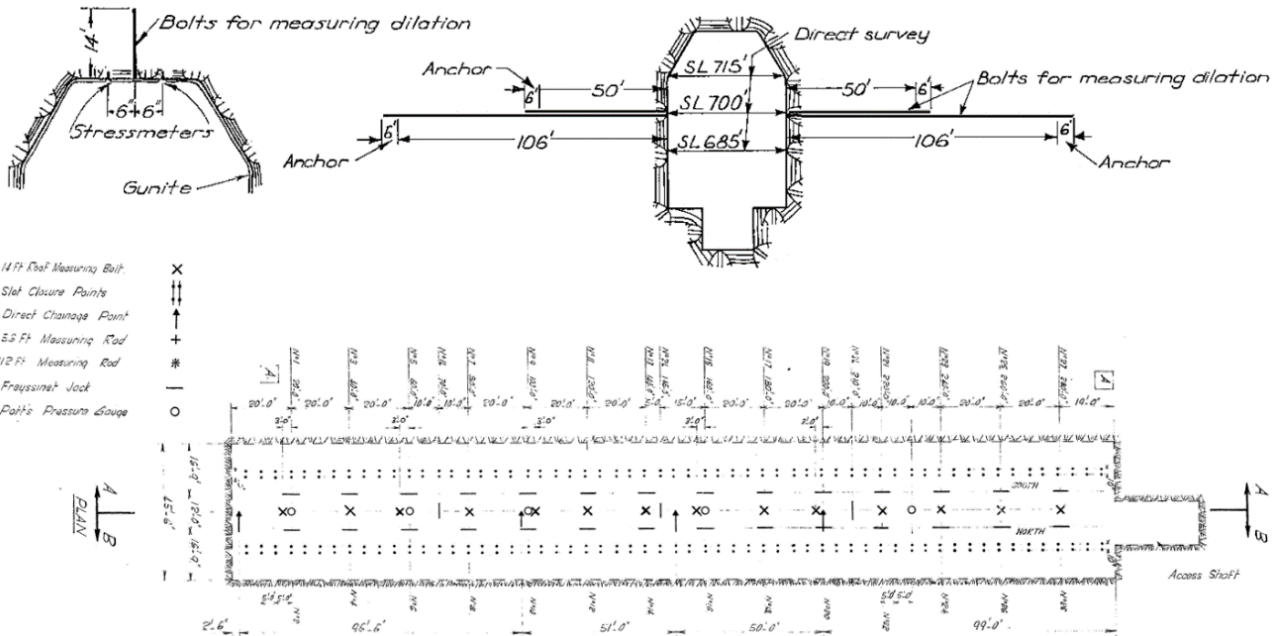


Figure 16: Monitoring instrumentation installed (modified after Endersbee and Hofto 1963)

During the initial stages of top heading excavation, prior to stress relieving being conducted, Endersbee and Hofto (1963) report that a shear failure developed at the intersection of the roof and the haunch on the southern side of the cavern. The failure being evident by a “feather edge on which a small relative movement could be seen” (e.g., slabbing). Coincident with the roof slabbing was a loud noise. In these cases, the roof was barred down but became drummy again after only 4-8 hours. It is reported that the roof continued to slab until 0.45 m of rock was removed but “drumminess” was still observed. At this stage in construction, the stress relieving commenced on the south side of the excavation. It proceeded

the north side by 3.8 m. Figure 18 presents the observed condition of the top heading in the initial stages of excavation. At this stage only 4.3 m bolts with a 0.9 m spacing were installed in the roof of the excavation. The unevenness of the roof profile indicates the instability reported is likely to have been caused by localised blast damage and is limited to the immediate roof bed.

When the top heading was advanced 28 m, a large failure occurred in the roof in front of the face, the stress relieving slots were 13.7 m behind the face (Endersbee and Hofto, 1963). After this point, stress relieving was advanced to 1.5 m behind the face and 3.7 m infill bolting was installed on a 0.9 m pattern.



Figure 17: Condition of Top Heading during early stages of excavation (Hydro Tasmania Archive)



Figure 18: Condition of top heading during late stages of excavation (Hydro Tasmania Archive)

Endersbee and Hofto (1963) state that the failure was attended by “a loud report accompanied by excessive slot closure” when one slot was inadvertently left unsealed (Stage 3 of Figure 2) for a distance of 7.5 m, and inspection with a periscope in holes drilled for rock bolts showed horizontal cracks of maximum thickness 1.6 mm, in the roof at 0.15 m, 0.6 m and 1.2 m above the roof surface. Rock bolts which had already been installed prior to the failure and which were overcored as part of the recent study showed a significant offset at a depth of 0.6 m above the roof. This appeared to have occurred prior to grouting, and indeed was observed in three rock bolts that were not grouted (Figure 19).



Figure 19: Deformation of grouted and ungrouted rock bolts in the cavern roof observed after overcoring

Figure 20 presents the response of the numerical model after 30 m advance of the Top Heading, prior to placement of the infill bolting described above. The model indicates the onset of shear displacement along bedding, primarily in the haunches of the trapezoidal roof. The residual low-level velocity in the model indicates that the roof and haunches are only marginally stable which is consistent with the in-situ observations by Endersbee and Hofto (1963) and the decision by engineers to install infill bolting and advance the stress relieving slot to within 1.5 m of the face.

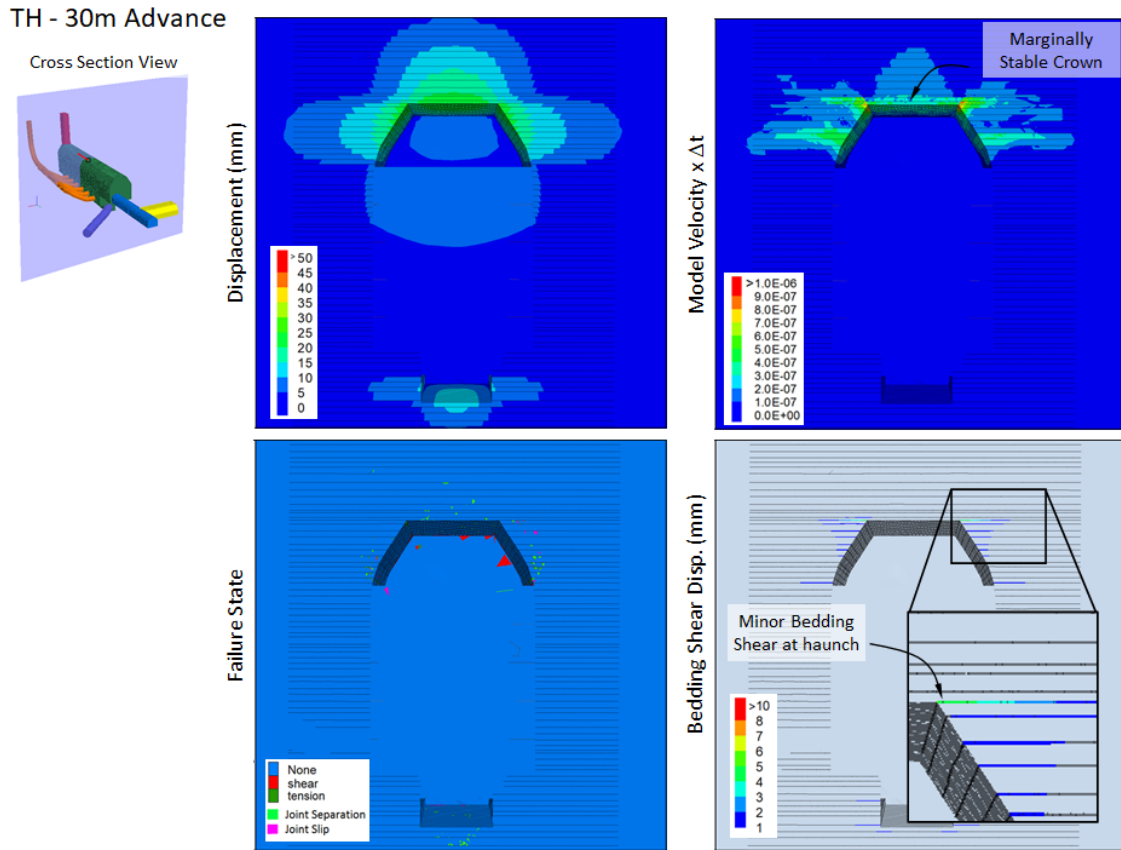


Figure 20: Model response after 30m Top Heading Advance

Prior to commencement of the stress relieving slot, Endersbee and Hofto (1963) report that flat jacks located 1.8 m on either side of the centreline gave an average stress of 29.6 MPa. After installation, the stress relieving slots reduced the roof stresses to 11.4 MPa and spalling was observed to cease. Within the model, the stress relieving slots have been simulated by reducing the normal stiffness of an explicit pre-defined plane. This reduction in normal stiffness represents the installation of a weak mortar. Figure 21 illustrates the induced horizontal stress perpendicular to the cavern before and after simulation of the stress relieving slot (29.6 MPa and 11.4 MPa respectively).

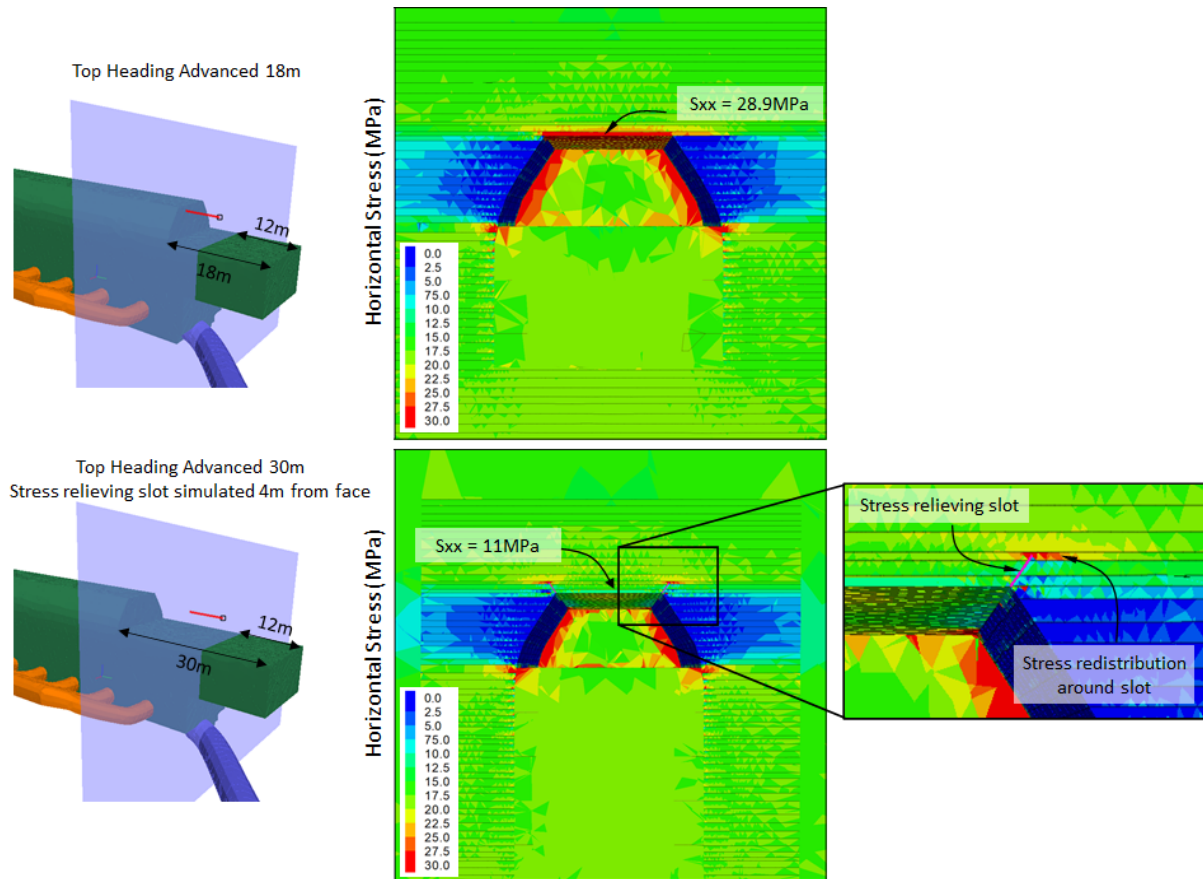


Figure 21: Initial development of horizontal stress within cavern roof

Figure 22 presents the response of the model after completion of the top heading and tailbay. The model indicates a stable cavern crown with minor shearing of bedding at the roof haunch and minor tensile yielding of the rock blocks. The model response is consistent with the increased stability documented (Figure 18).

Following excavation of the top heading and tailbay, the remainder of the cavern was excavated by benching down in 1.8 m – 2.4 m cuts. When the excavation was 13.7 m deep, Endersbee and Hofto (1963) report that a deep shear fracture developed at the intersection of the roof and haunch which was a continuation of the shearing observed during excavation of the top heading. The fracture occurred at the same time that the final bench between the main cavern and tailbay had become overstressed. Figure 23 illustrates the rock fracture in the floor of the main cavern.

Figure 25 presents the response of the model after completion of Bench 4. The model indicates a stable cavern crown with increased shearing of bedding at the roof haunch. Significant yielding and instability in the pillar between the main cavern and tail bay is simulated, which is consistent with the observed behaviour during excavation. Increased displacement is simulated at the intersection of the cavern roof and the shaft which is also consistent with the fracturing observed in the cavern floor during construction (Figure 23).

Figure 26 presents the response of the model after completion of the cavern which shows increased wall deformation and shearing of the explicit bedding partings. This response is consistent with observation of the final cavern configuration illustrated in Figure 23.

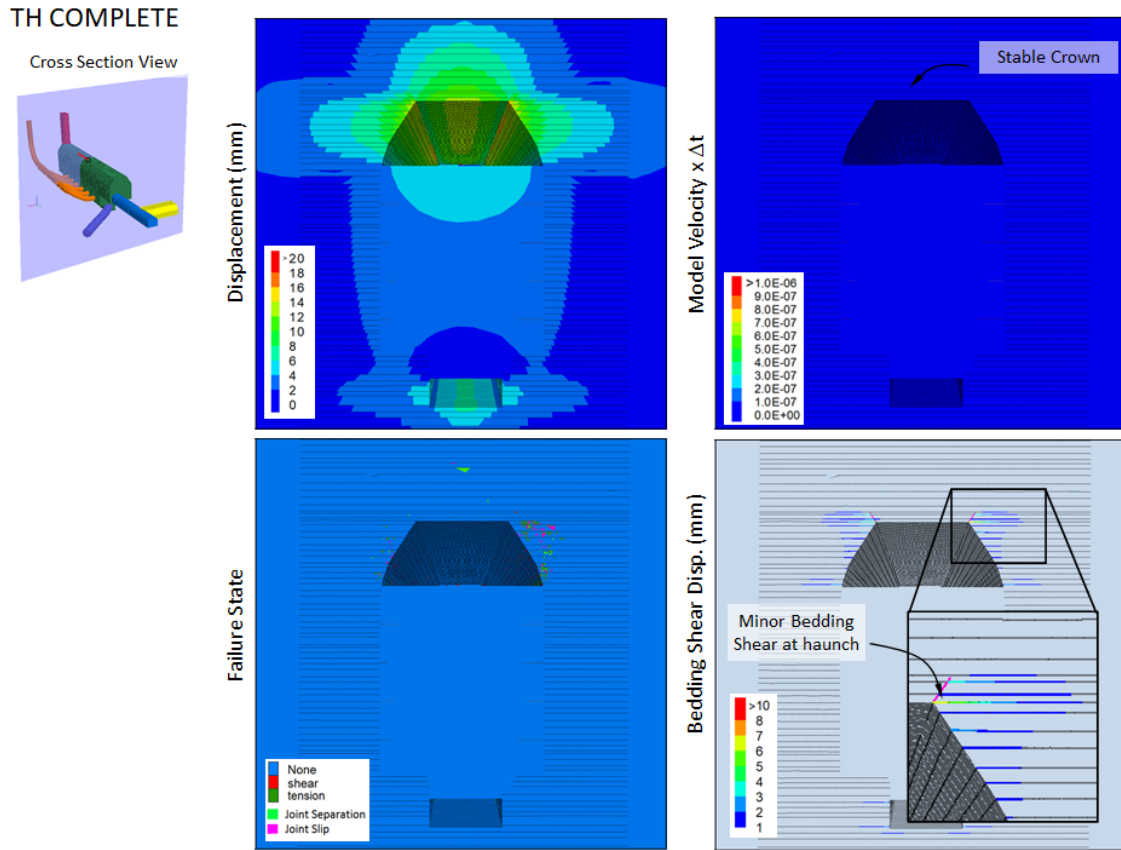


Figure 22: Model response after completion of the top heading and tailbay



Figure 23: Rock fracture in floor during cavern excavation (Endersbee and Hofto, 1963; Hydro Tasmania Archive)



Figure 24: Condition of final cavern excavation (Hydro Tasmania Archive)

B4 COMPLETE

Cross Section View

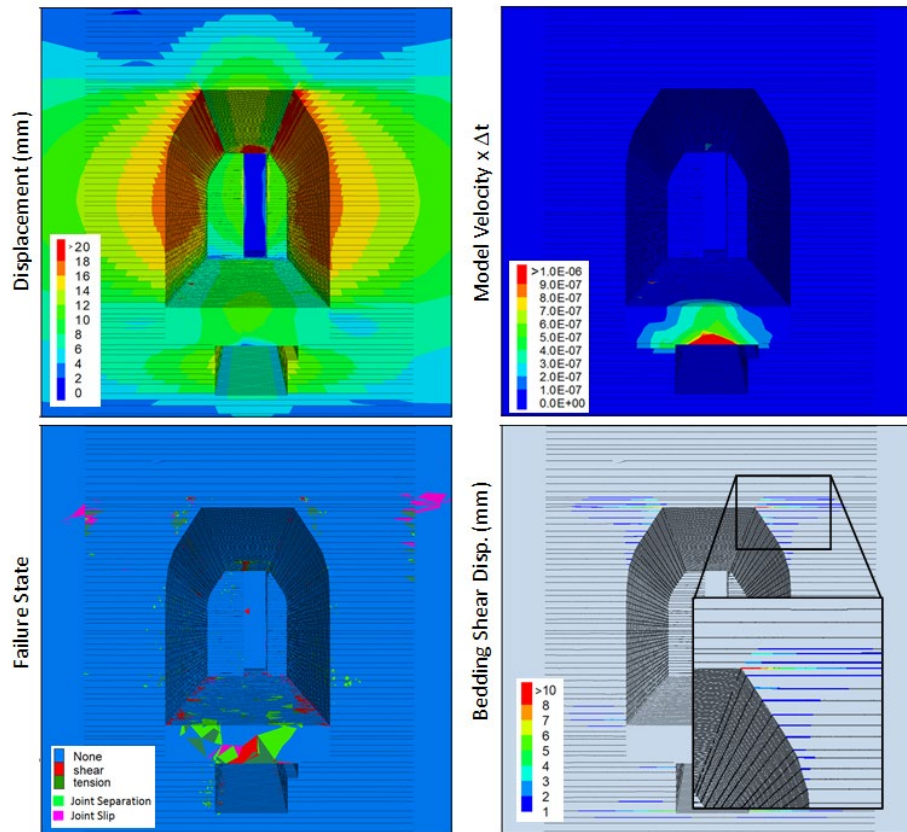
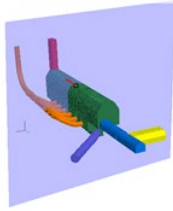


Figure 25: Model response after completion of Bench 4

CAVERN COMPLETE

Cross Section View

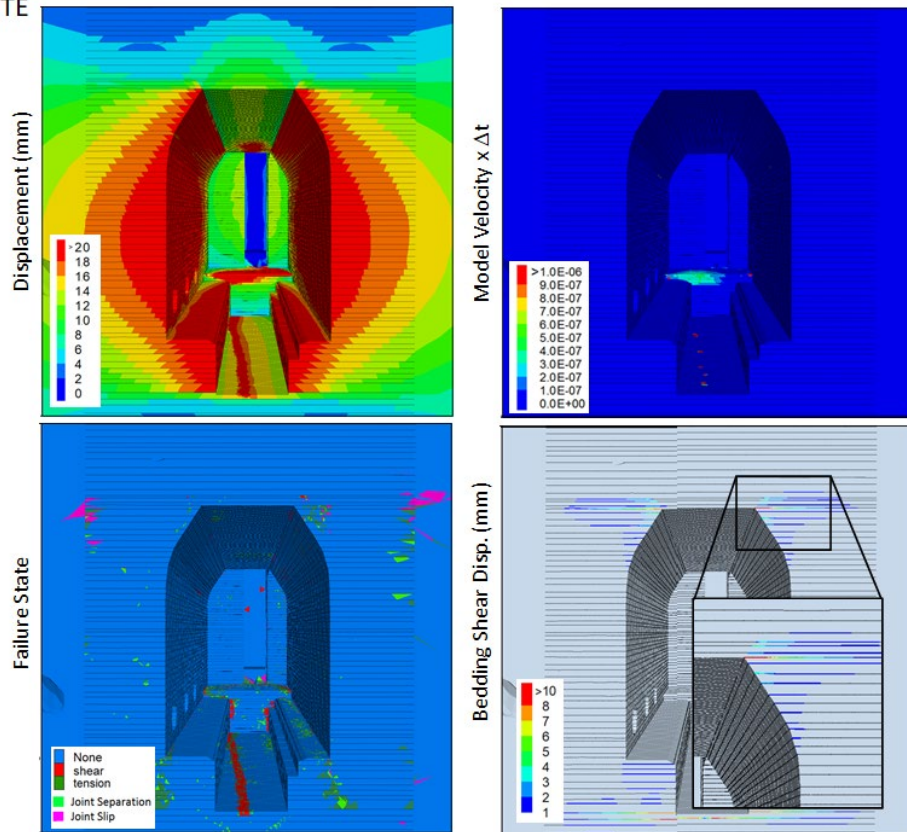
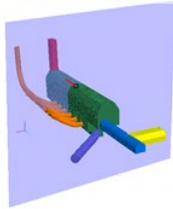


Figure 26: Model response after completion of the Cavern

3.1.2.1 Induced stress

The evolution of horizontal stress perpendicular to the cavern within the model is presented in Figure 27. As discussed, simulation of the stress relieving slots accurately reflects the stress reduction in the immediate cavern roof during excavation of the top heading. Stresses are observed to gradually increase during excavation of the remaining cavern due to stress redistribution.

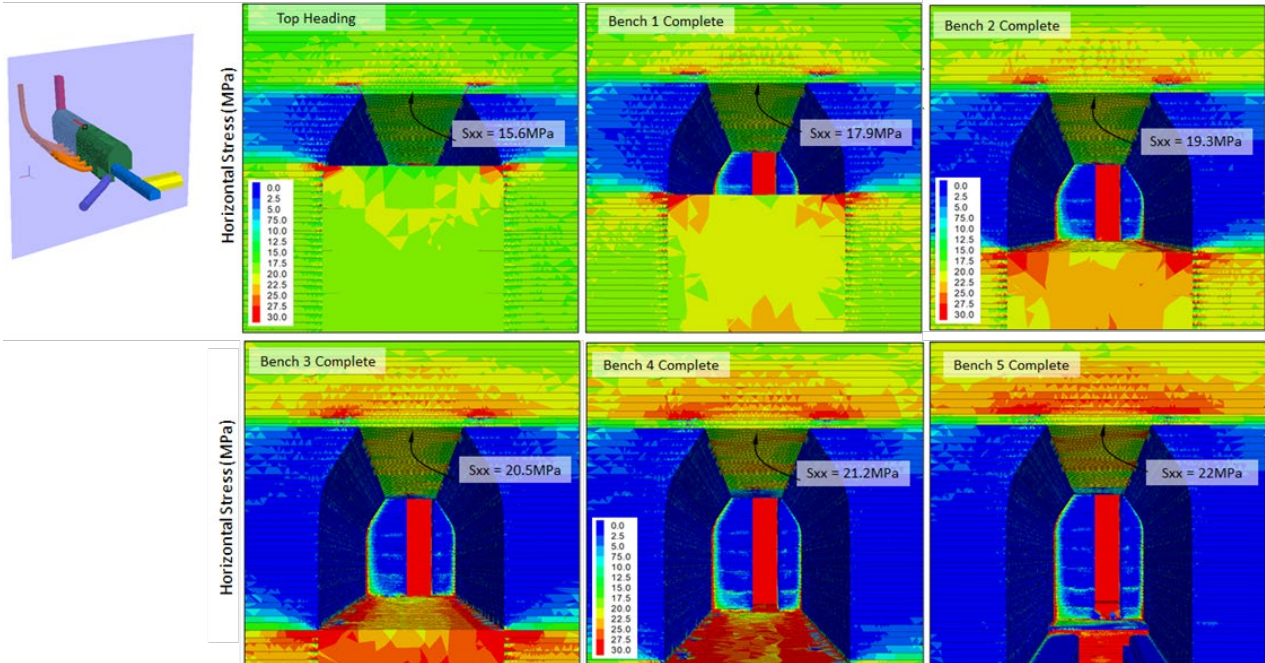


Figure 27: Evolution of horizontal stress throughout cavern excavation

Endersbee and Hofto (1963) present the average stress measured in all working flat jacks throughout excavation of the cavern. Figure 28 presents the measured stresses together with the modelled horizontal stress in the immediate roof bed in the centre of the cavern. The model provides a close match to the measured roof stresses throughout excavation of the entire cavern.

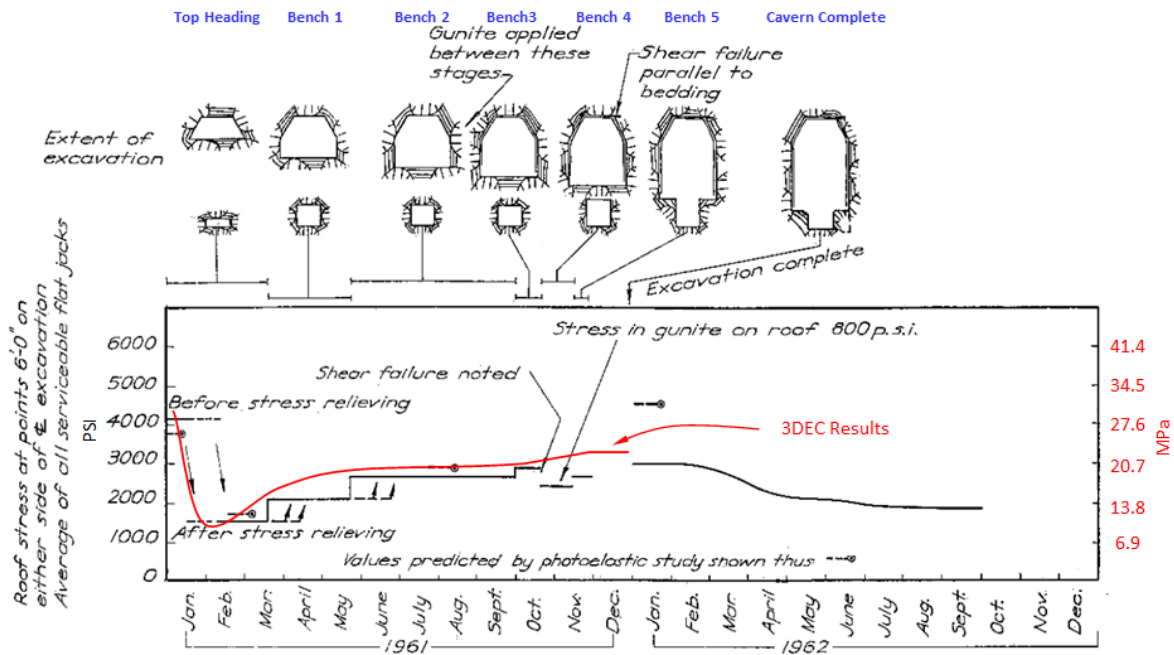


Figure 28: Comparison of measured and modelled horizontal stress (modified after Endersbee and Hofto, 1963)

3.1.2.2 Dilation and convergence

The average roof dilation measured in ungrouted roof bolts is presented in Figure 29 along with the modelled dilation at three locations. Considering the very low magnitude of dilation (< 5 mm) the model provides a close match to the measured dilation when the average of the discrete locations is considered.

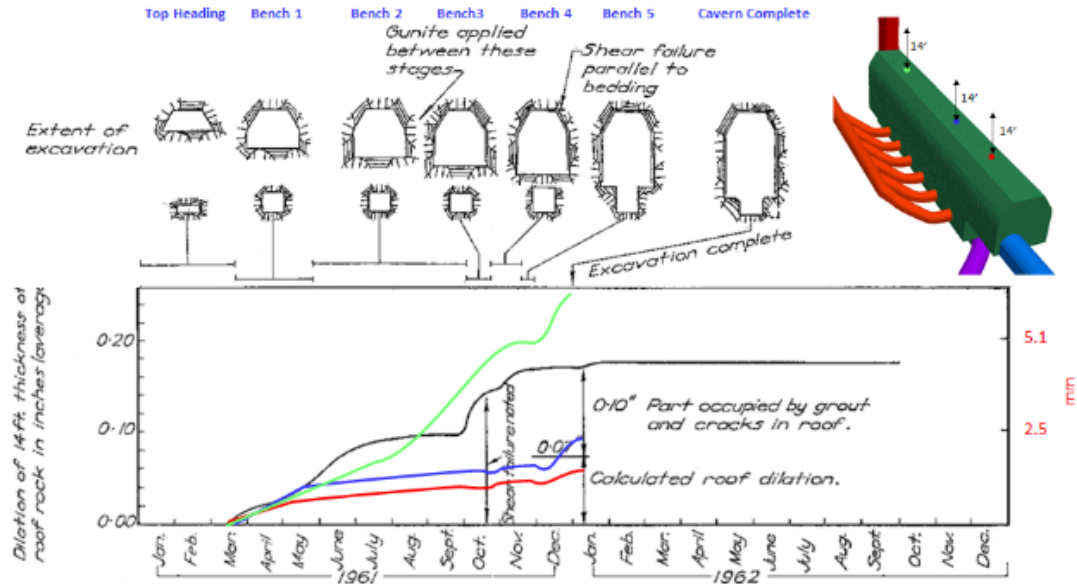


Figure 29: Comparison of measured and modelled roof dilation (modified after Endersbee and Hofto, 1963)

Dilation of the cavern sidewalls was measured at three locations along the cavern axis. Figure 30 presents the average values together with modelled dilation at centre of the cavern. Figure 31 presents the average measured sidewall convergence together with the modelled convergence at the SL 715' level and at the SL 700' level. In both cases, the model provides a very close match to the measured dilation.

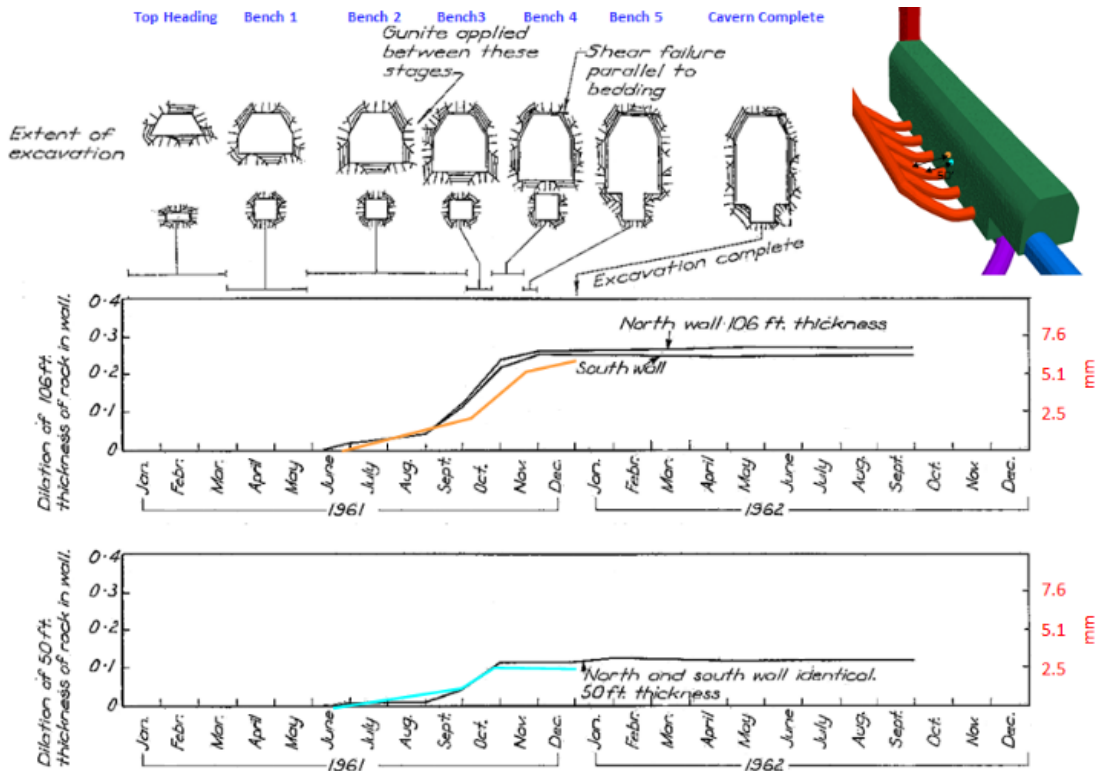


Figure 30: Comparison of measured and modelled sidewall dilation (modified after Endersbee and Hofto, 1963)

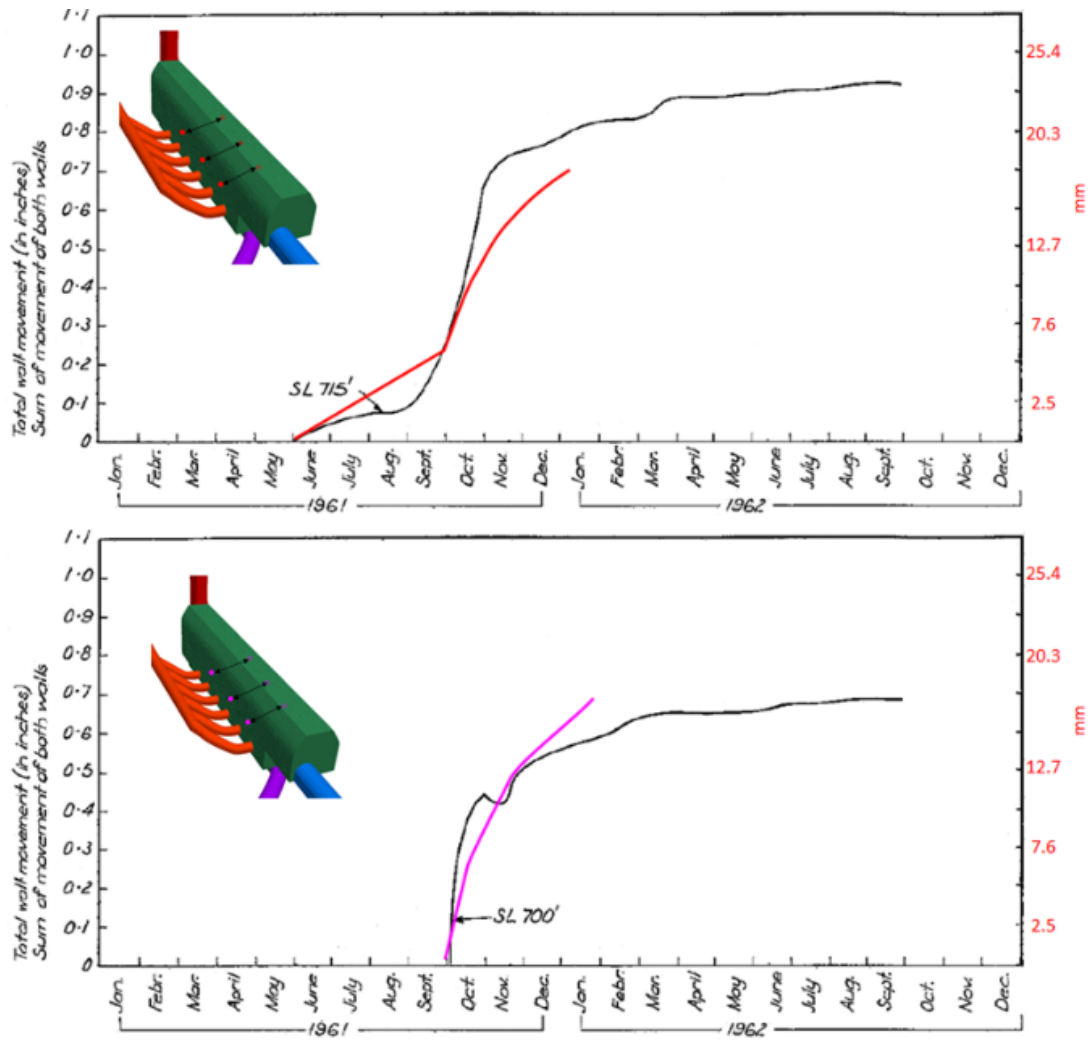


Figure 31: Comparison of measured and modelled sidewall convergence at SL 715': top and SL 700' : bottom (modified after Endersbee and Hofto, 1963)

3.2 GROUND SUPPORT RESPONSE

3.2.1 Rock bolts

The response of the simulated slot and wedge rock bolts after completion of the cavern is presented in Figure 32. The bolt state indicates some shear yield (dowel rupture) in the haunches of the trapezoidal roof which is consistent with the areas of predicted bedding shear observed in situ. However, the axial force within each bolt indicates the bolts are well below their maximum capacity (150 kN). Some grout yield is observed in the simulation in the haunches of the trapezoidal roof, while only minor local anchor yield is observed. These results are consistent with the stable conditions observed currently onsite.

3.2.2 Shotcrete (gunite) liner

The response of the 100 mm thick mesh reinforced shotcrete liner was considered at the completion of the simulated excavation and is presented in Figure 33. Only minor (< 10 mm) displacement is predicted in the sidewalls of the cavern. Tensile thrust forces (in the hoop direction) are predicted which are slightly higher on the southern (or upstream) side of the cavern above the penstock tunnels. These forces can be attributed to the straight wall design of the cavern, and some minor cracking in the liner could be expected and is observed.

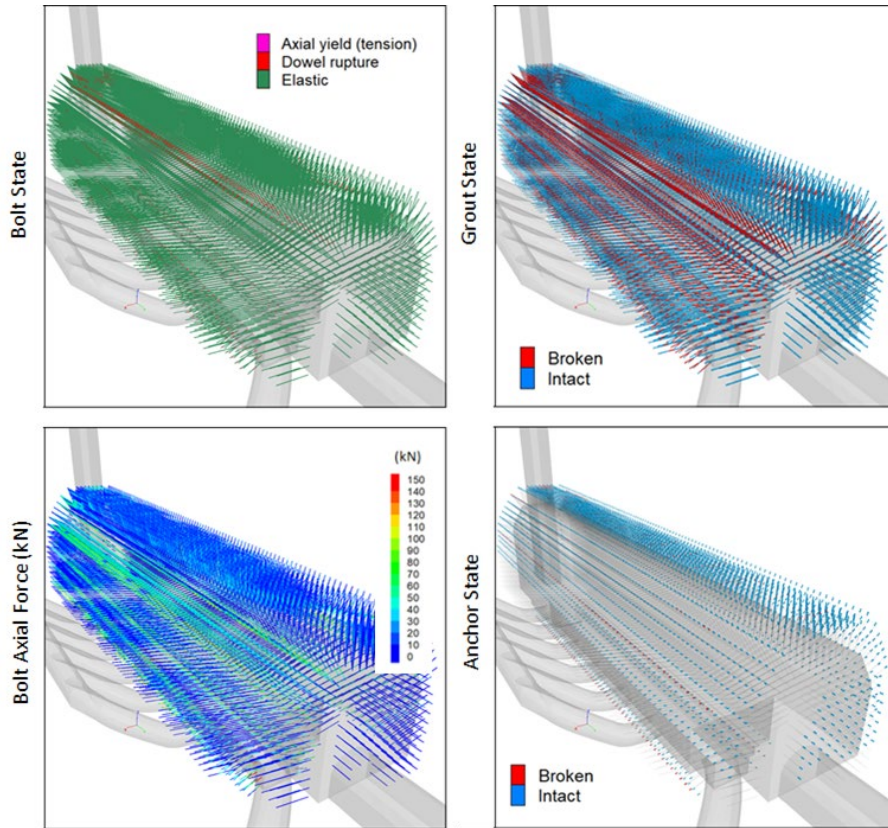


Figure 32: Rock bolt failure condition and axial force (left) and grout and anchor failure condition (right) after cavern excavation

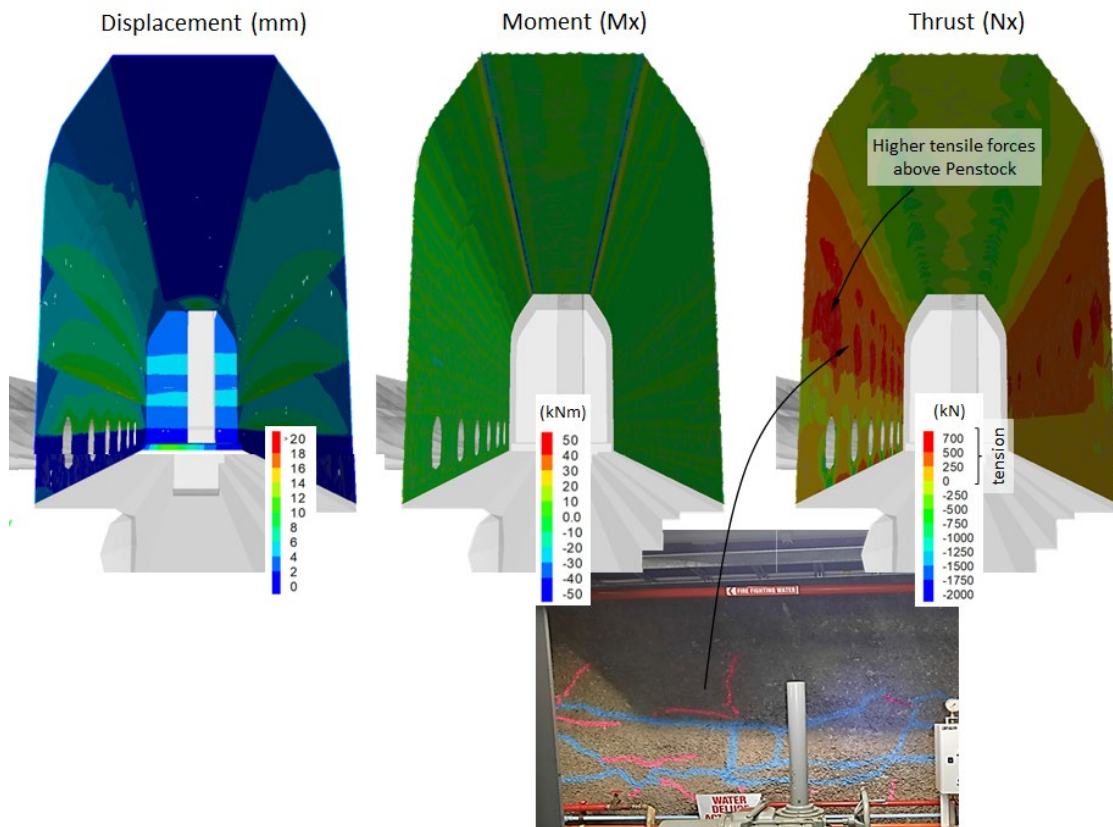


Figure 33: Mechanical response of shotcrete liner

3.3 CONSIDERATION OF FUTURE STABILITY OF CAVERN

Based on the results presented in Sections 3.1 and 3.2 it can be concluded that the model constructed provides an accurate representation of the historical and current geotechnical conditions in the cavern. As such, in order to assess the impact of potential long-term ground support degradation on the overall cavern stability, a series of models were analysed with progressive reduction in ground support capacity. Simulation of the degradation of all grout within the rock bolts and the shotcrete liner was predicted to result in negligible rock mass displacement and have no impact on cavern stability. Further simulation of potential bolt corrosion whereby 50 percent of the rock bolts were removed, together with all grout and the shotcrete liner, is predicted to result in only minor rock mass displacement. Simulation of the extreme case whereby all ground support elements are degraded to zero capacity is predicted to result in instability and collapse of the immediate roof beds throughout the cavern. However, the model does not predict instability within the cavern walls or large-scale propagation of the roof collapse.

4 CONCLUSION

Based on historical observation and monitoring data, a detailed three-dimensional numerical model of the construction of the Poatina Power Station Cavern has been developed. The model is able to provide an accurate representation of the observed ground conditions during construction that includes matching observed failure modes and measured induced stresses and displacements. Based on the model results, the stress relieving slots stress are observed to have decreased the maximum induced stresses within the haunches of the cavern roof and redistributed them to the tips of the slots promoting stability within the trapezoidal roof. Additional infill ground support installed during the initial excavation of the top heading was observed to be necessary and effective in stabilising shear failures along bedding structures during excavation of the cavern top heading. The current observed conditions within the cavern match with the simulated results.

In order to assess the impact of potential long-term ground support degradation on the overall cavern stability, a series of models were analysed with progressive reduction in ground support capacity. Based on the findings of these models, Hydro Tasmania was able to undertake a more informed review of the risks associated with the current ground support performance and cavern stability. Hydro Tasmania will continue the surveillance and monitoring program and the capacity of the ground support elements will be reviewed again with a view to install additional ground support if justified at the next major station outage currently scheduled for 2047.

5 ACKNOWLEDGMENTS

The authors would like to thank Hydro Tasmania for permission to publish this work. We would also like to acknowledge the pioneering rock mechanics research, design and construction conducted by the Hydro-Electric Commission of Tasmania. Particularly, Prof. Lance Endersbee and E.O. Hofto for their detailed and rigorous reporting and publication of the rock mechanics studies, observations and monitoring results from construction of the Poatina Cavern.

6 REFERENCES

- Ballantine R, Dalby K, Gobbart W (1965) Great Lake Power Development, Poatina and Arthurs Lakes Schemes-- Civil Construction. *J Inst Eng Aust* 7:93–113
- Barros JAO (1998) Experimental behavior of mesh reinforced shotcrete and steel fiber reinforced shotcrete panels. In: *core.ac.uk*. https://core.ac.uk/display/55613421?utm_source=pdf&utm_medium=banner&utm_campaign=pdf-decoration-v1. Accessed 1 Jan 2021
- Clark I (2006) Simulation of Rock mass Strength Using Ubiquitous Joints. In: Hart R, Varona P (eds) *Numerical Modeling in Geomechanics — 2006*; Proc. 4th International FLAC Symposium. Itasca Consulting Group, Madrid, p Paper No. 08-07
- Clarke M (1968) Geological Survey Record No. 7 - A reappraisal of a Lower Permian type section Golden Valley, Tas
- Colebatch G, LA E, Paxton H (1963) Discussion - Grouted Rock Bolts. *Proc Inst Civ Eng Geotech Eng* July-Augus:145–150
- Colebatch G, Tapping P, Hale G (1959) The Great Lake Power Development – civil engineering investigation and preliminary design. *J Inst Eng Aust* 31:85–100
- Cui Z, Sheng Q, Leng X (2016) Control effect of a large geological discontinuity on the seismic response and stability of underground rock caverns: A case study of the Baihetan #1 Surge Chamber. *Rock Mech Rock Eng* 49:2099–2114. <https://doi.org/10.1007/s00603-015-0908-6>
- Dasgupta BI (2000) Numerical Modeling of Large Underground Caverns for Hydro Power Projects. In: ASCE (ed) *Trends in Rock Mechanics :GeoDenver 2000*. Denver, pp 50–64
- Department of the Army US Army Corps of Engineers (1980) CECW-EG Engineer Manual 1110-1-2907 Engineering and Design : Rock Reinforcement. Washintgon DC
- Dickinson JC, Gerrard RT (1963) Discussion on Paper No 6703* Cameron Highlands hydro-electric scheme. *Proc Inst*

Civ Eng Geotech Eng 26:

- Endersbee L, Hofto E (1963) Civil Engineering Design and Studies in Rock Mechanics for Poatina Underground Power Station, Tasmania. *J Insitution* 35:129–208
- Ghorbani M, Sharifzadeh M (2009) Long term stability assessment of Siah Bisheh powerhouse cavern based on displacement back analysis method. *Tunn Undergr Sp Technol* 24:574–583. <https://doi.org/10.1016/j.tust.2009.02.007>
- Hoek E, Brown ET (1997) Practical estimates of rock mass strength. *Int J rock Mech Min Sci* 34:1165–1186
- Hu Z, Xu N, Li B, et al (2020) Stability Analysis of the Arch Crown of a Large-Scale Underground Powerhouse During Excavation. *Rock Mech Rock Eng* 53:2935–2943. <https://doi.org/10.1007/s00603-020-02077-4>
- Itasca Consulting Group (2022) 3DEC - Distinct-Element Modeling of Jointed and Blocky Material in 3D
- Kazakidis VN, Diederichs MS (1993) Understanding jointed rock mass behaviour using a ubiquitous joint approach. *Int J Rock Mech Min Sci* 30:163–172. [https://doi.org/10.1016/0148-9062\(93\)90709-M](https://doi.org/10.1016/0148-9062(93)90709-M)
- Lambe, TW (1973) Predictions in soil engineering. *Geotechnique* 23:151–202. <https://doi.org/10.1680/geot.1973.23.2.151>
- Li A, Liu Y, Dai F, et al (2020) Continuum analysis of the structurally controlled displacements for large-scale underground caverns in bedded rock masses. *Tunn Undergr Sp Technol* 97:103288. <https://doi.org/10.1016/j.tust.2020.103288>
- Moy D (1975) The design and monitoring of rock bolt and dowl systems in underground excavations. Imperial College of Science and Technology
- Pike G, Threder V, Moore W (1966) Geological Survey Explanatory Report : Zone 7 Sheet No 46 (8219N) Quamby
- Sainsbury B, Pierce M, Mas Ivars D (2008) Analysis of Caving Behaviour Using a Synthetic Rock Mass — Ubiquitous Joint Rock Mass Modelling Technique. In: SHIRMS. Perth
- Sainsbury B, Sainsbury D (2017) Practical Use of the Ubiquitous-Joint Constitutive Model for the Simulation of Anisotropic Rock Masses. *Rock Mech Rock Eng* 50:1507–1528. <https://doi.org/10.1007/s00603-017-1177-3>
- Sainsbury D, Amon A (2017) Advanced Analysis of Tunnel Excavation within the Anisotropic Melbourne Formation. In: 16TH Australasian Tunnelling Conference 2017. ATS, Melbourne
- Tang X, Rutqvist J, Hu M, Rayudu NM (2019) Modeling Three-Dimensional Fluid-Driven Propagation of Multiple Fractures using TOUGH-FEMM. *Rock Mech Rock Eng* 52:611–627. <https://doi.org/10.1007/s00603-018-1715-7>
- The Hydro-Electric Commission of Tasmania, Drawing A781, date unknown.
- Thompson AG, Villaescusa E (2014) Case studies of rock reinforcement components and systems testing. *Rock Mech Rock Eng* 47:1589–1602. <https://doi.org/10.1007/s00603-014-0583-z>
- Worotnicki, G, (1961) Photoelastic investigation of stress distribution in the rock around the machine hall of Poatina Underground Power Station, Tasmania, Report No. S.E. 49, Snowy Mountains Hydro-Electric Authority: Cooma.
- Yazdani M, Sharifzadeh M, Kamrani K, Ghorbani M (2012) Displacement-based numerical back analysis for estimation of rock mass parameters in Siah Bisheh powerhouse cavern using continuum and discontinuum approach. *Tunn Undergr Sp Technol* 28:41–48. <https://doi.org/10.1016/j.tust.2011.09.002>
- Yoshinaka R, Osada M, Park H, et al (2008) Practical determination of mechanical design parameters of intact rock considering scale effect. *Eng Geol.* <https://doi.org/10.1016/j.enggeo.2007.10.008>
- Zhang M, Zhu H, Zhu Y (2016) Stability analysis of blocks formed with determined joint network - A case study of Shenxu Caverns with 3DEC. In: Gomez, Detournay H& N (ed) Applied Numerical Modeling in Geomechanics. Itasca International Inc., Minneapolis, pp 435–443.